arXiv:1204.5110v1 [cond-mat.soft] 23 Apr 2012

Affine and Non-Affine Motions in Sheared Polydisperse Jammed Emulsions

J. Clara-Rahola[1],[*] T. A. Brzinski[1], D. Semwogerere[1], K. Feitosa[2],[†]
J. C. Crocker[2], J. Sato[3], V. Breedveld[3], and Eric R. Weeks[1‡]
[1]*Department of Physics, Emory University, Atlanta, GA 30322, USA*
[2]*Department of Chemical and Biomolecular Engineering,*
University of Pennsylvania, Philadelphia, PA 19104, USA and
[3]*School of Chemical and Biomolecular Engineering,*
Georgia Institute of Technology, Atlanta, GA 30332, USA
(Dated: March 3, 2013)

We study dense and highly polydisperse emulsions at droplet volume fractions $\phi \geq 0.65$. We apply oscillatory shear and observe droplet motion using confocal microscopy. The presence of droplets with sizes several times the mean size dramatically changes the motion of smaller droplets. Both affine and nonaffine droplet motions are observed, with the more nonaffine motion exhibited by the smaller droplets which are pushed around by the larger droplets. Droplet motions are correlated over length scales from one to four times the mean droplet diameter, with larger length scales corresponding to higher strain amplitudes (up to strains of about 6%).

PACS numbers: 83.80, 47.57.Qk, 83.85.Ei

Many materials behave as solids, despite having liquid-like amorphous structure. Obvious examples are glassy materials, which are disordered on an atomic scale [1]. Other examples include piles of sand, dense colloidal pastes, and shaving cream foams, which are disordered on the scale of microns or millimeters. Solids are characterized by their response to stress: they deform elastically (below a yield stress), rather than flowing. This behavior is well understood for crystalline materials, but somewhat more poorly for amorphous materials [1, 2]. In particular, most work has focused on the case of fairly monodisperse samples composed of particles all of similar sizes [3–15]. However, many natural materials of interest are highly polydisperse, with particle sizes varying by factors of ten or more. The rheology of such materials has been much less widely studied [16, 17]. There have been differences noted from the monodisperse case, such as a lower strain amplitude required for viscous flow [18] and diminished sample viscosity [19, 20]. The causes of these differences are not well understood.

In this Letter, we study highly polydisperse emulsions. Our emulsions are composed of oil droplets in water, stabilized by a surfactant, and are at sufficiently high volume fractions ($\phi \geq 0.65$) that the samples act as amorphous solids [17, 18, 20]. We subject the samples to low amplitude oscillatory shear and follow the droplet motion in the interior of the sample via confocal microscopy [10, 11, 21]. Most droplets rearrange elastically [5] and move sinusoidally. However, these motions are not necessarily affine, as shown in Fig. 1. In particular, our main finding is that in a highly polydisperse emulsion, the smaller droplets frequently undergo highly nonaffine droplet motion. In contrast to the shear of monodisperse samples [6, 10, 11, 14], the largest droplets allow for "cross-talk" between layers at different heights which have different mean velocities. The motions of droplets are correlated over large length scales, up to four times the mean droplet radius, with longer range correlations found for higher applied strain amplitudes.

We use the shear-rupture method of Ref. [22] to create decane-in-water emulsion droplets stabilized with SDS, skipping the fractionation step. The continuous phase is composed of a 65:35 volume ratio of water and glycerol to index match the decane droplets. Volume fractions are tuned to the range $0.65 \leq \phi \leq 0.85$ by centrifugation and dilution. Prior to our experiments, the samples are gently stirred to prevent any size segregation due to sedimentation, although for our high volume fractions sedimentation and size segregation are exceedingly slow.

We place the samples in a parallel-plate shear cell. The design is similar to that of Ref. [9] and our apparatus is described more fully in Ref. [11]. The gap of the cell is fixed at $H = 200$ μm. The lower glass plate does not move, whereas the top plate is driven sinusoidally at a frequency $f = 1$ Hz by a piezoelectric driver. The amplitude is $A = 40$ μm and therefore the macroscopic strain amplitude is $\gamma = A/H = 0.2$. Where the sample comes into contact with the glass plates, we add a coating of ScotchGard (3M). The sample wets the ScotchGard, pinning the sample to the coated region and ensuring a no-slip boundary condition at each plate. The oil droplets are deformable, but our experiments are conducted at volume fractions and strain amplitudes over which the droplets are fairly spherical.

The sample is imaged from below through the stationary plate using a confocal microscope. Fluorescein dye is added to the continuous phase to visualize the droplets as shown in Fig. 1. To quantify the size distribution of our system we acquire three-dimensional (3D) image stacks

---

[*] Current address: Department of Physics, Georgia Institute of Technology, Atlanta, GA 30332, USA.

[†] Current address: Dept. of Physics and Astronomy, James Madison University, Harrisonburg, VA 22807, USA.

[‡] Electronic address: erweeks@emory.edu

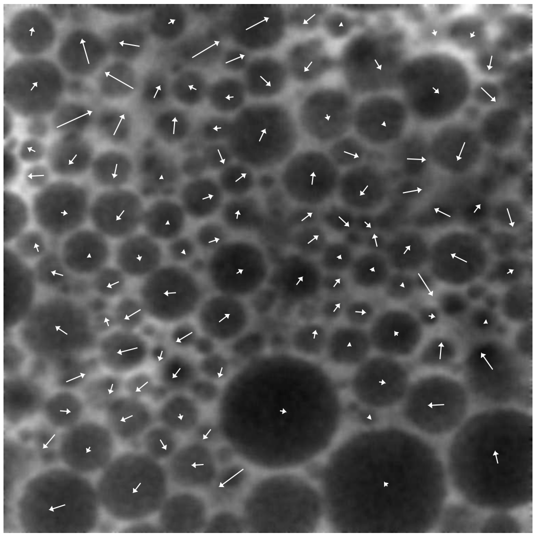

Figure 1: Confocal microscopy image of our polydisperse decane-in-water emulsion at $\phi = 0.65$. The arrows indicate the total displacement of each droplet from the peak-to-peak of one half oscillation cycle; they are twice the length of the true displacement, for easier visualization. The mean droplet displacement (2.8 μm to the left during the half-cycle) has been subtracted off from the displacement arrows. The image corresponds in time to the mid-point of this half-cycle. The width of the image is 56 μm and the arrows are to scale. The depth is $z = 24$ μm, the strain amplitude is $\gamma = 0.067$, and the volume fraction is $\phi = 0.65$.

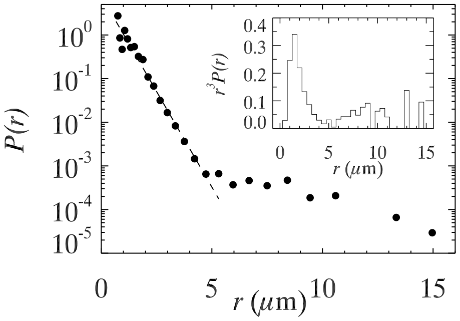

Figure 2: Probability distribution of droplet sizes in a $\phi = 0.80$ sample. Droplets with radius $r < 5$ μm are fit to an exponential (dashed line) with decay length 0.5 μm. The data for $r > 11$ μm correspond to only three observed droplets, and thus the true shape of the distribution is ill-defined for the larger droplets. The inset shows the same data, with the probability weighted by the droplet volume by multiplying by r^3. Note that the inset is plotted on a linear scale, while the main graph is plotted on a logarithmic scale.

from a static sample of size $56 \times 59 \times 80$ μm^3 at a vertical resolution of $\delta z = 0.1$ μm. To observe the dynamics when sheared, we must take data as rapidly as possible and thus we only use two-dimensional (2D) images. For the 2D experiments, images of size 56×59 μm^2 are acquired at a rate of 90 images per second for 33 s.

Using the 3D data from static samples, we determine the true droplet radii using custom software implementing the method of Ref. [23]. The size distribution obtained from this method is shown in Fig. 2. The average droplet radius is 1.2 μm, the standard deviation is 0.6 μm, and the Sauter mean radius $r_{32} = \langle r^3 \rangle / \langle r^2 \rangle$ is 2.3 μm. The data for small radii are reasonably well fit by an exponential with decay length 0.5 μm. However, there are a number of unusually large droplets with sizes larger than 5 μm. While these droplets are rare, they account for a nontrivial portion of the volume, as can be seen by the volume-weighted probability distribution shown in the inset to Fig. 2.

For 2D data analysis, we use a slightly different analysis technique. We identify droplets using the 2D-Hough transform [24], which lets us identify the droplets' radii and positions in each image. From that data, we then use conventional techniques to track their corresponding trajectories [25]. Both standard tracking and the iterative image tracking technique described in Ref. [21] are used to reconstruct each trajectory. Note that for each droplet, because our observation is only in 2D, we do not know the true radius $r_{3\mathrm{D}}$. However, we observe that due to the curvature of the interfaces, droplets are not distinguishable in 2D slices when they are viewed more than $\Delta z \approx 0.6 r_{3\mathrm{D}}$ away from their center, and so for each droplet, the droplet radius r we apparently observe is in the range $0.8 r_{3\mathrm{D}} < r \le r_{3\mathrm{D}}$.

When an oscillatory strain is applied to the emulsion, the majority of droplets rearrange reversibly and periodically at the driving frequency. The average velocity field is $v(z,t) = \gamma z \sin(2\pi f t)\hat{x}$. The largest droplets ($r \gtrsim 8$ μm) move sinusoidally at this mean velocity; this is reflected by the very short displacement vectors drawn on the largest droplets in Fig. 1. In contrast, smaller droplets move in a variety of directions. Some move affinely with the applied shear, but many move in other directions, as shown in Fig. 1. This behavior is likely due to the largest droplets. At the equator of a large droplet, it moves with the expected velocity for that height z. However, droplets tend to move coherently as spheres (rather than deforming), and thus the top of a large droplet moves with an amplitude γr too small relative to the expected velocity at height $z + r$. Likewise, at height $z - r$ the large droplet is moving more quickly than the mean velocity for that height. Thus, two large droplets that are nearby but with centers at different z values do not have the same velocities, and as they move back and forth sinusoidally, they push and pull on the smaller droplets between them. These smaller droplets thus have apparently random motions. In practice, the larger droplets are rarer and thus less likely to influence each other. Moreover, they move based on the average influence of the smaller droplets surrounding them, and so their motion is likely to tend to average velocity field. The contrast in motion between large and small droplets in a polydisperse sample is the main conclusion of this

ϕ	$\gamma_{\rm loc}$	$z_0[\mu m]$	$\xi_x[\mu m]$	$\xi_y[\mu m]$
0.65	0.070	-9.0	9.4	10.3
0.70	0.102	-13.8	14.7	9.1
0.75	0.054	-9.2	8.0	9.6
0.85	0.070	-8.8	8.3	11.7

Table I: Volume fraction ϕ, observed local strain amplitudes $\gamma_{\rm loc}$ for different volume fractions ϕ; observed slip length z_0; and the characteristic length scales ξ_x and ξ_y. The macroscopic applied strain amplitude is 0.20 for all experiments. The uncertainties for all listed lengths are ±0.3 μm.

Letter. This differs qualitatively from cases where large-scale flows cause non-affine motion, and which typical require large amplitude strain [7, 14].

Over the 33 s movies, approximately 8% of the droplets make an irreversible rearrangement at some point. This only occurs with smaller droplets, $r <\sim 5$ μm. Before and after the irreversible rearrangement, the droplets move periodically. The rarity of plastic rearrangements in our data is similar to a prior study of a more monodisperse emulsion [5].

At this point we only study droplets whose trajectories are reversible (elastic) and thus periodic. We respectively denote as $x(t)$ and $y(t)$ the components of a trajectory parallel and perpendicular to the shear axis at time t. A least squares fit is applied to each component with functional forms:

$$\begin{aligned} x(t) &= a_x \sin(\omega t + \theta_x) \\ y(t) &= a_y \sin(\omega t + \theta_y) \end{aligned} \qquad (1)$$

where $\omega = 2\pi f$, using the known value of the driving frequency f. The fit parameters a_x and a_y give the amplitudes of the periodic motions of the droplet, and θ_x and θ_y are phases. These functional forms provide a good fit to the particle trajectories.

We study the sample at depths $z = 24, 36, 48$, and 60 μm, relative to $z = 0$ defined at the stationary bottom plate. At each height we compute the mean amplitude $\langle a_x \rangle$. We find $\langle a_x \rangle \sim \gamma_{\rm loc} \cdot (z - z_0)$ where $\gamma_{\rm loc}$ is the local strain amplitude and z_0 is a slip length. $\langle a_x \rangle$ does not extrapolate to 0 at $z = 0$, but rather at negative values ranging from $z_0 = -8$ to -14 μm. The local strain is always smaller than the applied strain. This suggests that the emulsion partially slips at the top plate, or possibly has a shear band somewhere where the local strain is significantly higher. See Table I for further information about each particular experiment. We do not observe the behavior of purely slipping emulsions in any of our experiments [26].

The distributions of the fitting parameters a_x, a_y, θ_x and θ_y are quite broad, as shown in Fig. 3. While many droplets move with the mean amplitude $\langle a_x \rangle$ as appropriate for that height, several have amplitudes that differ by 0.5 μm or more from the mean. Negative values of $a_x - \langle a_x \rangle$ indicate droplets moving with smaller amplitudes than might be expected, and likewise positive values indicate droplets moving with larger amplitudes.

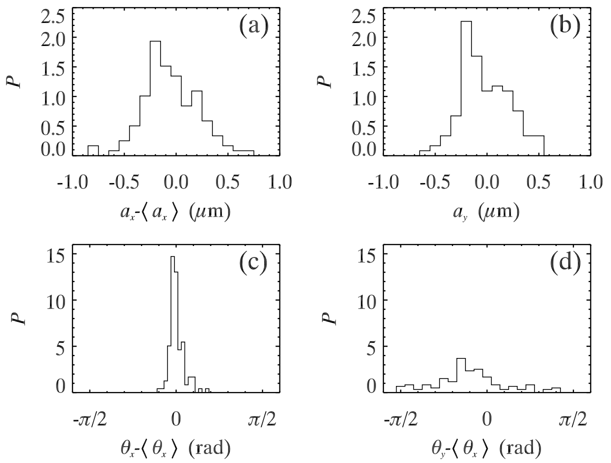

Figure 3: Probability distributions of the fit parameters. These are (a) amplitudes of the parallel components, (b) amplitudes of the perpendicular components, (c) phase angles of the parallel components and (d) phase angles of the perpendicular components of the trajectories. Data correspond to a $\phi = 0.65$ emulsion at a local oscillatory strain amplitude $\gamma = 0.070$, at a depth $z = 24$ μm. The data for $P(a_x)$ are centered around $\langle a_x \rangle = 2.4$ μm. The means for the phase angles are arbitrary as they depend on when we set $t = 0$, although note that the distribution for θ_y is centered around the mean value of θ_x. The lack of symmetry in these distributions is due to observing a finite number of droplets.

These results are equally true in the direction of the applied strain [Fig. 3(a)] and perpendicular to this direction [Fig. 3(b)], showing many droplets have significant nonaffine motion. The amplitudes associated with big droplets are found at the central peaks of $P(a_x)$ and $P(a_y)$. The outliers are more likely to be associated with smaller sized droplets, with the tails of the distribution coming from some of the smallest droplets with $r \sim 1$ μm. Note that a_y from our fits (Eqns. 1) is positive: to get values $a_y < 0$, we assume that all droplets move in phase, and so droplets with phase angles θ_y that appear π out of phase with the dominant motion are adjusted, $a_y \to -a_y, \theta_y \to (\theta_y - \pi)$. In general we find $\langle a_y \rangle \approx 0$, as expected by symmetry.

The phase angles also vary from droplet to droplet. In the direction parallel to the shear, most droplets move in phase, as $P(\theta_x)$ is peaked and narrow as shown in Fig. 3(c). In contrast, $P(\theta_y)$ is broadly distributed around a central peak, as shown in Fig. 3(d). The phase angle in y ranges up to $\pi/2$ away from the average phase, indicating some droplets move periodically but completely out of phase with the driving strain.

To understand the spatial character of the particle behavior, we construct images with each droplet positioned at its time-averaged position, and color coded based on its motion, shown in Fig. 4. The color scale corresponds to the value of a_x (left) and a_y (right). The biggest droplet has a color corresponding to the center of the

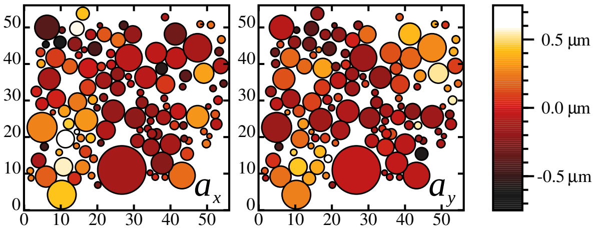

Figure 4: (Color online) Droplets which move elastically, drawn at their mean position. The color code indicates the parallel (left picture) and perpendicular (right picture) amplitude of each droplet. The color bar denotes the amplitude scale in μm, where 0 denotes the average amplitude for these data ($\langle a_x \rangle = 2.4$ μm, and using 0 μm for the a_y data). The images correspond to the data shown in Fig. 3.

color scale, in other words, it is moving with the average motion of all droplets. The droplets moving with anomalous amplitudes corresponding to the extremes of the color scale are the smaller droplets. Droplets with similar a_x or a_y tend to be close together.

To gain further insight into the spatial clustering of droplets with similar characteristics, we identify droplet pairs which are separated by a surface-to-surface distance Δr, that is, droplets separated by a center-to-center distance $r_{12} = r_1 + r_2 + \Delta r$, where r_i is the radius of droplet i in the 2D image. Then, we compute the Pearson correlation coefficient of the amplitude a_x:

$$C(\Delta r) = \frac{1}{N(\Delta r)} \sum_{\langle i,j \rangle} \frac{(a_{x_i} - \langle a_x \rangle)(a_{x_j} - \langle a_x \rangle)}{\sigma_{a_x}^2} \qquad (2)$$

where $N(\Delta r)$ is the number of neighboring droplets, and a_{x_i} and a_{x_j} are the x-amplitudes of droplets i and j. The average $\langle a_x \rangle$ is for all droplets comprised by $N(\Delta r)$ and σ_{a_x} corresponds to the variance of the distribution of a_x. The choice of using the surface-to-surface distances rather than center-to-center is perhaps not obvious. However, each individual droplet moves as a solid object, thus completely correlated with itself (distances $r_{12} < r_1$). Examining the surface-to-surface motion lets us avoid considering this artificially correlated solid-body motion, and instead probe the properties of the effective medium between droplets. If we consider center-to-center separations, the results are noisy and do not have a simple dependence on the distance.

Figure 5(a) shows these correlation functions for a_x (solid symbols) and a_y (open symbols), for one sample at two different strain amplitudes. The correlation functions exhibit exponential decay with decay lengths in the range of 8-15 μm; the decay lengths for different samples are listed in Table I. These lengths are comparable to the sizes of the larger droplets in the sample. Figure 5(a) shows that correlations in the larger strain case (squares) decay slower than than in the small strain case (circles). We find ξ_x and ξ_y depend on $\gamma_{\rm loc}$ as shown in Fig. 5(b) for this $\phi = 0.65$ sample. Given the dependence of ξ on $\gamma_{\rm loc}$, it suggests that perhaps the variation we see for samples with different ϕ is perhaps more due to the variability in $\gamma_{\rm loc}$ for those data; see Table I.

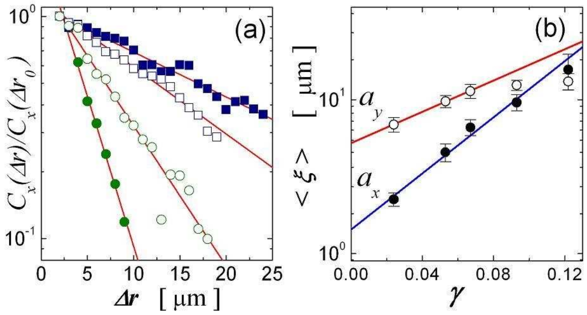

Figure 5: (Color online) (a) Spatial correlation functions of the droplet amplitudes a_x (solid symbols) and a_y (open symbols). The strain amplitudes are $\gamma_{\rm loc} = 0.017$ (circles) and $\gamma_{\rm loc} = 0.085$ (squares). The correlation functions are normalized by their value at $\Delta r_0 = 2$ μm. The data are from the same sample as Figs. 3 and 4. (b) Values of the exponential decay length scale for this sample as a function of strain amplitude, for correlations of a_x (solid symbols) and a_y (open symbols). The uncertainty of γ is 6%. The error bars are the standard deviations found from multiple experiments. All data for both panels of this figure are taken at depth $z = 24$ μm. The lines are guides to the eye.

We have studied jammed polydisperse emulsions, and observed highly complex droplet motion when our samples are sinusoidally sheared. Most droplets move periodically, but different droplets have different amplitudes and phases of their motion. The large droplets greatly rearrange the small droplets, although nearly all of this motion is reversible. We find length scales over which the droplet motions are correlated. These length scales range from 1 to 4 times the average droplet diameter, with the largest values found for the highest strains (up to strains of ∼ 0.08). Overall, our results suggest that the rheological response of highly polydisperse systems has a complex microscopic origin: larger droplets cause long-range correlations in the dynamics, while smaller droplets are like an effective fluid. Theoretical descriptions derived for less polydisperse systems will likely not apply or need to be modified [3, 6].

We thank G. W. Baxter, R. Besseling, C. Crane, R. Gonzalez, C. Hollinger, and W. C. K. Poon for helpful discussions. Funding from the National Science Foundation (grants DMR-0603055 and DMR-0804174), the Petroleum Research Fund (administered by the American Chemical Society, grant 47970-AC9), and the Swiss National Foundation (grant PBFR2-116930) is gratefully acknowledged.

---

[1] C. A. Schuh, T. C. Hufnagel, and U. Ramamurty, Acta Materialia **55**, 4067 (2007).

[2] L. Bocquet, A. Colin, and A. Ajdari, Phys. Rev. Lett. **103**, 036001 (2009).

[3] A. J. Liu, S. Ramaswamy, T. G. Mason, H. Gang, and D. A. Weitz, Phys. Rev. Lett. **76**, 3017 (1996).

[4] T. G. Mason, M. D. Lacasse, G. S. Grest, D. Levine, J. Bibette, and D. A. Weitz, Phys. Rev. E **56**, 3150 (1997).

[5] P. Hébraud, F. Lequeux, J. P. Munch, and D. J. Pine, Phys. Rev. Lett. **78**, 4657 (1997).

[6] M. L. Falk and J. S. Langer, Phys. Rev. E **57**, 7192 (1998).

[7] R. Yamamoto and A. Onuki, Phys. Rev. E **58**, 3515 (1998).

[8] W. Losert, L. Bocquet, T. C. Lubensky, and J. P. Gollub, Phys. Rev. Lett. **85**, 1428 (2000).

[9] G. Petekidis, A. Moussaïd, and P. N. Pusey, Phys. Rev. E **66**, 051402 (2002).

[10] P. Schall, D. A. Weitz, and F. Spaepen, Science **318**, 1895 (2007).

[11] D. Chen, D. Semwogerere, J. Sato, V. Breedveld, and E. R. Weeks, Phys. Rev. E **81**, 011403 (2010).

[12] M. V. Hecke, J. Phys.: Cond. Matt. **22**, 033101 (2010).

[13] J. R. Seth, L. Mohan, C. A. Locatelli-Champagne, M. Cloitre, and R. T. Bonnecaze, Nature Materials **10**, 838 (2011).

[14] M. B. Sexton, M. E. Mobius, and S. Hutzler, Soft Matter **7**, 11252 (2011).

[15] V. Chikkadi and P. Schall, Phys. Rev. E **85**, 031402 (2012).

[16] H. Princen, J. Colloid Interf. Sci. **112**, 427 (1986).

[17] A. Saint-Jalmes and D. J. Durian, J. Rheo. **43**, 1411 (1999).

[18] S. R. Derkach, Adv. Coll. Int. Sci. **151**, 1 (2009).

[19] R. Pal, AIChE J. **42**, 3181 (1996).

[20] R. Pal, Curr. Op. Coll. Int. Sci. (2010).

[21] R. Besseling, L. Isa, E. R. Weeks, and W. C. K. Poon, Adv. Coll. Int. Sci. **146**, 1 (2009).

[22] T. G. Mason and J. Bibette, Phys. Rev. Lett. **77**, 3481+ (1996).

[23] R. Penfold, A. D. Watson, A. R. Mackie, and D. J. Hibberd, Langmuir **22**, 2005 (2006).

[24] D. Ioannou, W. Huda, and A. F. Laine, Image and Vision Computing **17**, 15 (1999).

[25] J. C. Crocker and D. G. Grier, J. Colloid Interf. Sci. **179**, 298 (1996).

[26] S. P. Meeker, R. T. Bonnecaze, and M. Cloitre, Phys. Rev. Lett. **92**, 198302 (2004).